Infrared Physics & Technology 115 (2021) 103703

Contents lists available at ScienceDirect

Infrared Physics and Technology

journal homepage: www.elsevier.com/locate/infrared

Optical grating and THz polarizer based on normal grade single crystal diamond fast fabricated by fs laser

Baichuan Lin [a], Qi Song [a], Dongqing Pang [a,*], Bowen Liu [a], Weipeng Kong [b], Zeyu Li [b], Yu Qin [b], Minglie Hu [a]

[a] Ultrafast Laser Laboratory, Key Laboratory of Opto-electronic Information Technology (Ministry of Education), College of Precision Instrument and Optoelectronics Engineering, Tianjin University, 300072 Tianjin, China
[b] Research Center of Laser Fusion, China Academy of Engineering Physics, Mianyang 621900, China

ARTICLE INFO

Keywords:
Femtosecond laser
Normal grade single crystal diamond
Phase transition
Grating
Micrometer electric wire
THz polarizer

ABSTRACT

In this paper, we have researched the fs laser induced the phase transition in the normal grade single crystal diamond plates. The results show that the optical properties and electric properties of the irradiated region closely relate to the degree of the phase transition. We have succeeded in fabricating the optical gratings on the surface and inside of the diamond plates even though only partial material in the irradiated region phase-transforms from single crystal phase to amorphous phase. The gratings can be used as terahertz polarizers likewise. The modulation depths are 53% at 1.6 THz and 40% at 2.52 THz, which can be further improved by optimizing the fabrication parameters and the fill factors of gratings. We have also fabricated the electric wire on the surface of the normal grade diamond plate.

1. Introduction

Diamond has unique mechanical, thermal, chemical and optical properties that make it attract great interest in many applications [1,2,3]. Diamond material is difficult to process in the traditional way, so that pulse lasers become a suitable tool [4,5]. Nitrogen-vacancy defects in diamond can produced by 1 kHz, 226 nm [6] and 1 kHz, 790 nm [7] femtosecond laser. The polycrystalline diamond photonic waveguides can be realized by femtosecond laser lithography [8]. Pulse lasers can easily induce a diamond to graphite or amorphous carbon phase transition in the irradiated micrometer region in a single crystal diamond film or plate [9]. The electrodes have been fabricated on single crystal CVD diamond so called electronic grade diamond with the nitrogen content at the level of below 5 ppb by nanosecond pulse laser [10] and below 0.05 ppm by femtosecond pulse laser [11]. The micrometer electric wires have been written inside single crystal diamond film by 1 kHz, 800 nm, 100 fs Ti:sapphire laser [12].

A metal grating can be used as terahertz (THz) wave polarizer,[13] which can be fabricated by many methods, for examples, photolithography and wet etching,[13] nanoimprint technology [14] and femtosecond laser additive manufacture [15]. The THz wave modulation devices made of diamond have been rarely reported,[16] partly because the above-mentioned studies were always employed by using low repetition pulse laser with low scanning velocity inside expensive high purity diamond samples. This impedes practical applications of diamond devices due to low processing speed and high price.

In this paper, we studied the laser-induced phase transitions of relatively cheap diamond plates with the nitrogen content of 50 ppm by employing high repetition femtosecond fiber laser. The transmittance of the irradiated area in visible wavelength range always changes largely whatever the phase transition is complete or not. So we can freely fabricate the optical devices made of single crystal diamond plates. We have succeeded in fabricating the gratings both on the diamond surface and inside of the diamond plates. The experimental results show that the total diffraction coefficients are almost no difference between using the surface grating and using the inner grating. However, the electric properties are very sensitive to the degree of the phase transition and only completely amorphous carbon phase can provide a high conductivity in a 2 mm-long micrometer wire. Beyond our expected, the terahertz polarizer with the modulation depth of more than 53% at 1.6 THz can be also obtained even though the phase transition is not complete and electric conductivity is much less than the value of the electric wire. Our experimental results have demonstrated that the high repetition femtosecond laser is a powerful tool to fabricate electromagnetic wave

* Corresponding author.
E-mail address: pangdongqing@tju.edu.cn (D. Pang).

https://doi.org/10.1016/j.infrared.2021.103703
Received 16 January 2021; Received in revised form 25 February 2021; Accepted 28 February 2021
Available online 23 March 2021

elements in single crystal diamond at a relatively high speed.

2. The experimental setup

The experimental setup for femtosecond laser fabrication is shown in Fig. 1. The laser system was a homemade 1040 nm, 500 kHz, 270 fs, 2 W Yb-doped photonic crystal fiber amplifier. The lenses of L1 and L2 were used to enlarge the beam diameter and minimize the angle of divergence. The focus length of L1 is 40 mm and that of L2 is 80 mm. Through them the $1/e^2$ spot diameter is about 2.8 mm. An objective lens (NA = 0.4) was used to focus the laser pulses on the sample, which was placed on a computer-controlled 3D translation table. A confocal microscope was used to monitor the real-time manufacturing process. The model of the 3D stage is Newport ESP300 and the minimum moving distance is 0.1μm.

The primary samples are the single crystal diamond plates (type 2a) synthesised by microwave plasma assisted chemical vapor deposition (MPCVD), which is provided by Carbon Six Science and Technology Co., Ltd., China. The primary samples used in our experiments are normal grade of single crystal diamond with the nitrogen content of 30–50 ppm. The cross section is 3mm × 3mm and the thickness is 0.3 mm. The primary samples are colorless and transparent in the whole visible range. The total transmittance of a 0.3 mm-thick plate at 633 nm is about 72% including the loss of surface reflections. The phase transition of the irradiated regions were studied by Raman spectrometer (RENISHAW-inVia).

3. The studies of the phase transitions

The optical properties of a diamond plate are sensitive to the chemical bonds and only single crystal diamond with pure sp^3 bonds can be transparent in very wide range, including the visible, infrared and terahertz wavelength. The melting and resolidification process induced by the ns laser [17] or the fs laser [12] can result in the generation of a great deal of sp^2 bonds and the transformation from the single crystal phase to amorphous carbon phase in the laser-irradiated region. Fig. 2 shows the microscope images of separated lines written with three typical parameters (see Table 1). The laser power of several tens milliwatt was just beyond the threshold of the phase transition for obtaining the minimum line width. For the typical scan velocity of 1 mm/s, more than 200 pulses were deposited on one point.

As Fig. 2 shows, the optical properties of the fabricated regions are sensitive to the processing parameters in the case of the low power. All three samples change color after the laser fabrication but the gray levels of three samples are obviously different. The line fabricated on the surface of the diamond plate looks light black and the line inside seems a little lighter than the surface line. The color of Sample black becomes dark black since the line was scanned three times by the laser. The color variations of three samples illustrate that the phase transition is strongly influenced by the fabrication condition, not only usual parameters such as laser power and scanning velocity, but also the scanning times and the depth of the irradiated region, especially when we minimized the laser power.

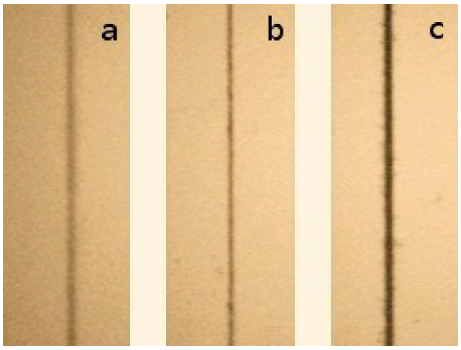

Fig. 2. The separated lines fabricated at different parameters. (a) Sample surface, (b) Sample inner, (c) Sample black.

Table 1
Separated lines fabricated with different parameters, the depth is calculated with the refractive index of 2.4.

Sample name	Laser power	Scan velocity	Times	Position
surface	50 mW	1 mm/s	1	on surfae
inner	55 mW	1 mm/s	1	120 μm depth
black	150 mW	0.1 mm/s	3	on surface

Raman spectroscopy is most sensitive to highly symmetric covalent bonds with little or no natural dipole moment, for examples, the carbon–carbon bonds in single crystal diamond, graphite and amorphous carbon. It can provide a wealth of information about their structure and the phase transition. We measured the Raman spectra of the primary diamond plate and above-mentioned three samples excited by a 532 nm laser with 0.5% percent of power.

The summary of Raman spectra in the range of 200 to 3500 cm^{-1} is shown in Fig. 3 and the below-discussed peaks are labeled with the peak positions. A single sharp peak at 1332 cm^{-1} corresponding to the vibration of the sp^3 diamond lattice. The so-called G band, which lies at around 1560 cm^{-1} for amorphous carbon,[18] is due to the graphitization sp^2 bonds. A wide G band always occurs in the Raman spectra curves of all fabricated samples but the peak positions are a little different. This demonstrates that the laser fabrication process always leads to some degree of the phase transition from single crystal diamond

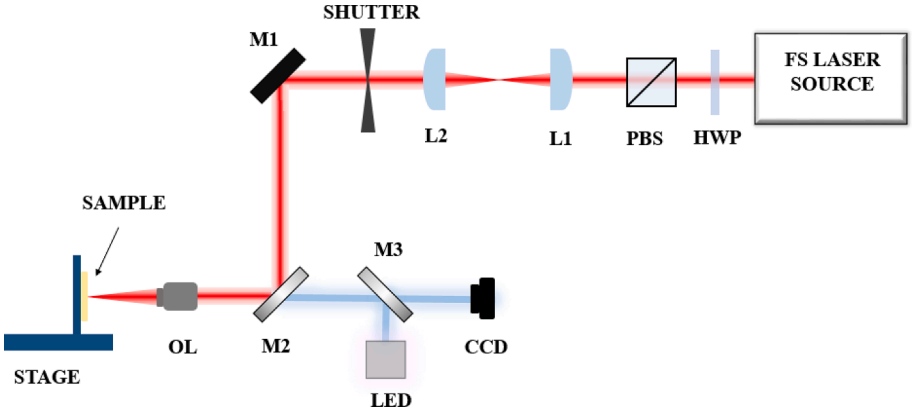

Fig. 1. The femtosecond laser micro-manufacturing system. LED: light emitting diode, CCD: coupled charge devices, PBS: polarization beam splitter, OL: objective lens, 3D stage: three-dimensional translation stage.

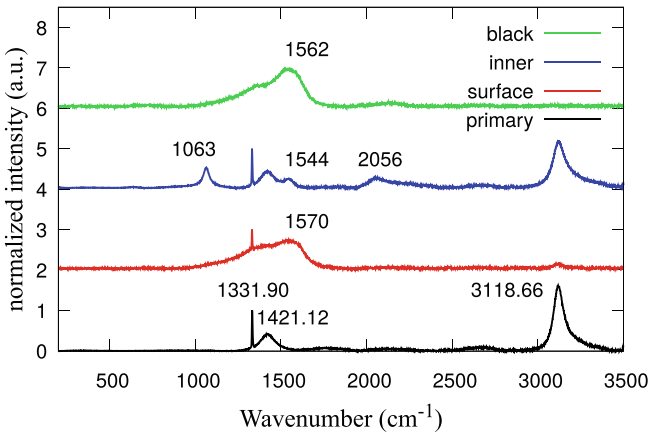

Fig. 3. The summary of Raman spectra of the primary sample and three typical fabricated samples.

phase to graphite phase or amorphous carbon phase. The wide band with a high peak at around 3119 cm^{-1} is due to the nitrogen and hydrogen impurities, and the intensity of this band is proportional to the nitrogen content [19]. Comparing the Raman spectra of Sample inner (the blue line) with others, the laser-induced phase transition inside the diamond plate is more difficult than on the surface mainly due to the high pressure. The existence of nitrogen atoms may also have some influence on the difficulty of the phase transition.

To focus on the variation of the C-C bonds, the Raman spectra in the region of 1100 to 1600 cm^{-1} are fitted with Gaussian curves. The primary sample consists of highly uniform C-C bonds in a tetrahedral crystal structure, so that a separate sharp peak at 1331.9 cm^{-1} is observed in its Raman spectra (see Fig. 4), which is assigned to the long-range order sp^3 bonds of a single crystal diamond [19]. The fitting curve gives that the full width at half maximum (FWHM) of the sharp peak is 4.79 cm^{-1} for the primary sample with the nitrogen content of 30–50 ppm. Near this sharp peak, there is a wide band with the peak at 1421 cm^{-1}, which is assigned to the distorted sp^3 bonds caused by hydrogen defects [19,20]. The G band does not exist in the Raman spectra of the primary sample. It means that the sample is single crystal diamond and there are no sp^2 bonds at all.

Fig. 5 shows the Raman spectra of Sample surface. The great change of the Raman spectra of Sample surface is the occurrence of a high, wide G band with the peak at 1570 cm^{-1}, which shows the phase transition from single crystal phase to graphite phase or amorphous carbon phase with the generation of a great deal of sp^2 bonds. There is a broad shoulder at 1000 to 1500 cm^{-1} containing the D band. If ignoring the sharp sp^3 peak in Fig. 5, the Raman curve of Sample surface is a typical Raman spectra of amorphous carbons with both the distorted sp^3 and sp^2 bonds without long range order [21,22,23]. The curve shape depends on the local structures of these sp^2 and sp^3 bonds [22]. The area ratio of the

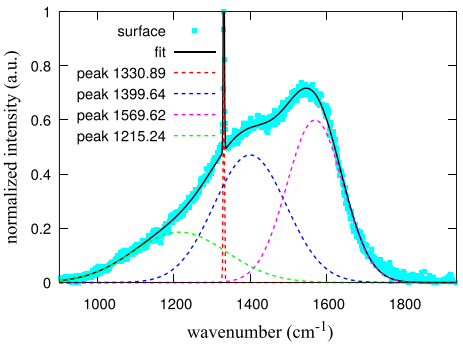

Fig. 5. The Raman spectra of Sample surface with curve fitting results.

G band sp^2 bonds is 39%.

The sharp peak of the sp^3 bonds also occurs in the Raman curve but the peak position shows a little red shift, from 1331.9 cm^{-1} to 1330.89 cm^{-1}. The FWHM of this peak drops to 3.33 cm^{-1}. The downshift of the peak suggests that the lattice stress changes after the phase transition. The existence of this sharp peak, which is attributed to the long range order sp^3 bonds, illustrates that the phase transition of the irradiated region is incomplete or nonuniform, namely, there is still part material in the form of single crystalline phase.

As well, the band above 3000 cm^{-1} almost disappears (see the red line in Fig. 3). There are many explanations, for examples, the decrease of the nitrogen content due to ultrafast annealing caused by high repetition fs laser, the H- or O-terminated sample, and the nitrogen atoms become interstitial atoms but the Raman spectra depends on the bonds. We are not sure which one is right or major due to limited measurement technologies. We didn't try to find and discuss the dynamics about the nitrogen atoms in this paper since it is beyond our purpose and it has no influence on our conclusions.

Sample black has been scanned three times at much slow velocity and its Raman spectra varies evidently. The sharp peak of the sp^3 bonds totally vanishes and the long range order of C-C bonds is lost, as Fig. 6 shows. The Raman curve only contains the wide G band with the peak at 1549.89 cm^{-1} and the wide shoulder from 1000 to 1500 cm^{-1} containing the D band. The area ratio of the G band sp^2 bonds is 59%. The phase transition becomes uniform and the color of the fabricated region displays dark black. In next section we will show how important the disappearance of the sharp peak of the sp^3 bonds is to fabricate a micrometer electric wire.

The phase transition becomes as well as different when the fabricated region is inside the diamond plate because the phase transition takes place in a high pressure condition. As Fig. 7 (a) shows, the G band still occurs and the peak position is 1543.51 cm^{-1}, but a separate, high, and sharp peak of sp^3 bonds displays that the phase transition is much inhibited in this situation. A high proportion of the bonds of the material in the fabricated region remains the long range order sp^3 bonds as in the

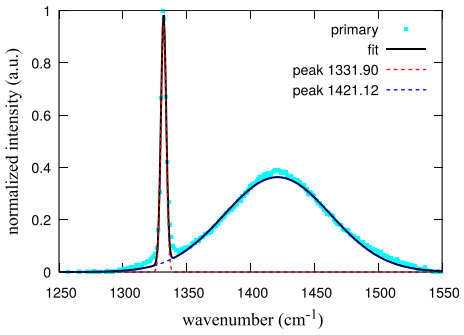

Fig. 4. The Raman spectra of the primary sample with curve fitting results.

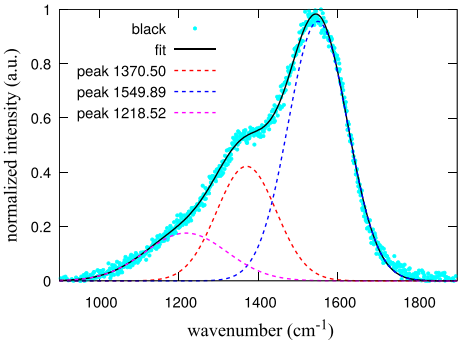

Fig. 6. The Raman spectra of Sample black and the fitting curves.

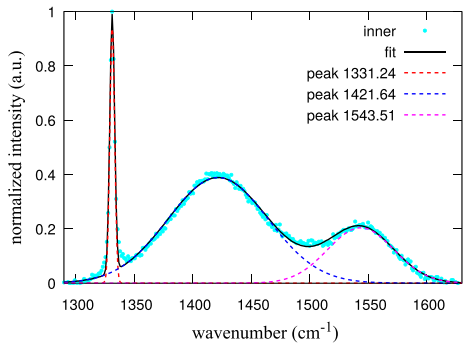

Fig. 7. The Raman spectra of Sample inner and the fitting curves.

single crystal diamond lattice. The area ratio of the G band sp^2 bonds is 24%.

For the inside fabrication, the N atoms can change their positions at high pressure, so that a portion of the C-N bonds varies the properties accordingly. It results in that the new bands containing a high peak at 1063.06 cm^{-1} occur in the Raman spectra as the blue line in Fig. 3 shows. These additive bands are assigned to the C-N bond when the nitrogen atom does not exist in the form of N-V centers [19,20]. This also causes the variations of the FWHM and the position of the sharp peak of the sp^3 bonds in Fig. 7. The FWHM becomes 4.84 cm^{-1}, which is very close to that of the primary sample, 4.79 cm^{-1}, and the peak position becomes 1331.24 cm^{-1}, which is larger than that of Sample surface, 1330.89 cm^{-1} and smaller than that of the primary sample, 1331.89 cm^{-1}. The position and the FWHM of this sharp sp^3 peak are directly influenced by the lattice stress. They also contain the information on the nitrogen content and the properties of the C-N bonds.[24]

In summary, the phase transition is incomplete in the case of single scanning. For obtaining the complete amorphous carbon phase the multi-scanning is necessary when keeping the laser power low for a narrow line width. In next section, our experimental results show that the completeness of the phase transition is not a impediment factor for fabricating electromagnetic wave devices, whatever a optical grating or a THz grating polarizer. But, for obtaining a electric wire with high electric conductivity, we do need to the complete phase transition indicated by the removal of the sharp peak of the sp^3 bonds in the Raman spectra because it will retard the drift motion of free electrons through the whole wire.

4. Fabricating the optical grating, the micrometer electric wire and the THz wave polarizer

We processed gratings on the surface and inside of the diamond plates at the velocity of 1 mm/s. The grating periods are listed in Table 2. All samples were cleaned in the ultrasonic cleaning bath of acetone solution before the scanning electron microscope (SEM) and diffraction experiments. Fig. 8 (a) displays the SEM image of the grating on the surface and Fig. 8 (b) shows the optical microscope image of the grating inside the substrate. The lines are straight and the edges of the lines are very abrupt for both the surface grating and the inside grating. The line widths of the surface gratings are about 3 μm and those of the inner gratings look similar.

Table 2
List gratings on the surface and inside of diamond.

Sample name	laser power	Grating period	Position
s-10	50 mW	10 μm	on the surface
s-20	50 mW	20 μm	on the surface
s-40	50 mW	40 μm	on the surface
i-4	55 mW	4 μm	120 μm depth
i-10	55 mW	10 μm	120 μm depth
i-20	55 mW	20 μm	120 μm depth
i-40	55 mW	40 μm	120 μm depth

To evaluate the optical properties of the fabricated grating, we performed optical diffraction experiments with a He-Ne laser. A 632.8 nm laser was vertically incident on the gratings. A camera was used to record the diffraction patterns on the wall behind the samples. The diffraction angles were measured and the grating period can be calculated. The calculated period of each grating is exactly the same as the line spacing of the laser scanning. Fig. 9 (a) and (b) show the diffraction patterns of two gratings with the same period of 10 μm, one is fabricated on the surface and another inside of the diamond plate. The diffraction patterns are exactly alike. Fig. 9 (c) shows the dispersion spectra of the white light diffracted by the grating with period of 10 μm. It will be a good dispersion element.

The total diffraction efficiencies are also nearly the same if considering the surface reflection effect of the inner grating (see dark red line in Fig. 10). For examples, the total diffraction efficiency of the surface grating with period of 10 μm is 56.45% and that of the inner grating is 54.83%. As well, Fig. 10 also shows the intensity ratios of the first, second, third order diffraction of the gratings, cyan, yellow and green bars, respectively. The difference of the energy distributions between the surface grating and the inner grating results from that the line widths are a little different. There are very shallow grooves of the surface samples due to slight surface ablation, however, their effect can be neglected. The diffraction efficiency ratios can be further optimized by adjusting the grating parameters and the scanning design.

For the fabrication parameters of the surface grating, there is a sharp peak of the sp^3 bonds in the Raman spectra (see Fig. 5), which is related to long-range order of single crystal diamond lattice. As Fig. 2 shows, the laser irradiated region displays a dark gray (or light black) color. In this case, the phase transition is not complete from single crystal diamond phase to amorphous carbon phase. Especially, for the fabrication parameters of the inner grating, the degree of the phase transition of the material in the irradiated region is much less than the surface grating case. There is only a small portion of the phase transition. However, the diffraction patterns are alike and the total diffraction coefficients are almost identical. The diffraction experimental results demonstrate that the incompleteness and nonuniformity of the phase transition are not important for the performance of the optical grating in the visible range. The color of the diamond changes, which means the transmittance of the light drops greatly. So that we can use a normal grade single crystal diamond plate to fabricate the optical element, which can be designed freely and fabricated quickly by a high repetition fs laser. Such optical elements inside diamond is useful in the extreme environment due to excellent acid and alkali resistance of diamond.

However, the residual single crystal diamond phase is important for fabricating micrometer electric wire. We fabricated 2 mm long lines on the surface and inside of the substrate by using the same parameters as Sample black. The tracks of three scannings must exactly overlap. On the surface, two contact electrodes of dimension $100 \times 100 \mu m^2$ were fabricated for measurement. The resistivity is measured and calculated using the same method in Reference [12]. The voltammetric curve of the wire on the surface is shown in Fig. 11. The results show a sharp difference between the surface line and the inside line. The resistivity of the surface line drops tremendously by five orders of magnitude, from 60 Ωm to 4×10^{-4} Ωm. The resistivity of the surface line becomes close to the resistivity of amorphous carbon 5×10^{-5} Ωm and that of polycrystalline graphite 1.5×10^{-5} Ωm[25]. For the inside wire, the measured current is submerged in a noisy background because it is very close to the leakage current of the device. The obviously separate sharp peak of the sp^3 bonds in the Raman spectra of Sample inner (Fig. 7) means that only a small part of the material in the fabricated region transforms to amorphous carbon phase. Due to the existence of single crystal phase, the inner micrometer wire is almost nonconducting since the free electrons cannot drift through the whole wire when they are

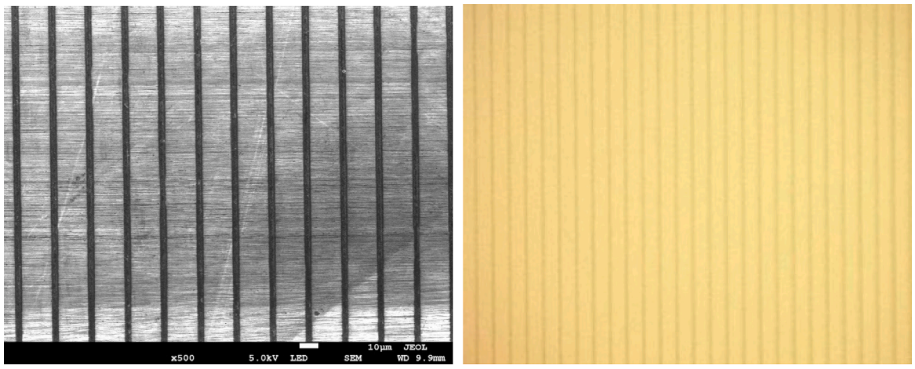

Fig. 8. (a) The SEM image of the surface grating whose period is 20 μm and (b) the optical microscope image of the inner grating.

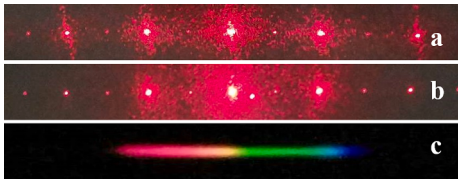

Fig. 9. The diffraction patterns the gratings with period of 10 μm. (a) the surface grating, (b) the inner grating, (c) the dispersion spectra of the white light.

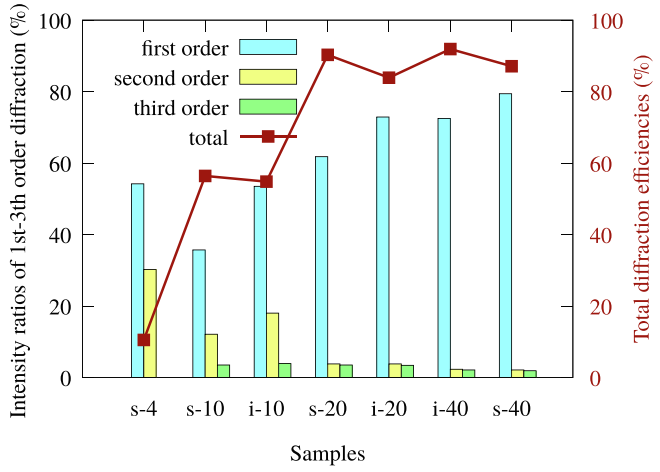

Fig. 10. The intensity ratios of the first, second, third order diffraction and the total diffraction efficiencies of the gratings at 632.8 nm.

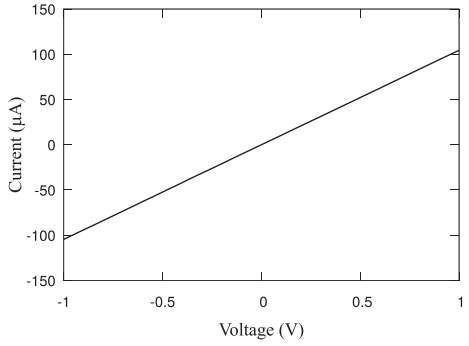

Fig. 11. The voltammetric curve of the micrometer electric wire on the surface.

driven by electric field. As well, the results also show that the exact overlap of the tracks of mutli-scannings is a major factor to obtain the high conductivity when keeping the width of the wire very narrow. It gives us opportunity to adjust the electric property and fabricate electric elements and practical electric circuits on the surface or inside of a diamond plate by using fs laser.

The results are beyond our expected when these gratings were used as THz polarizers. The measurement was carried out by using tunable single frequency linearly polarized THz source and the intensities were directly measured by the power meter (Golay Cell Tydex Gc1D). The result is the average value of more than three measurements. The modulation depths of Sample s-10 is 53% at 1.6 THz, calculated by $(I_{max} - I_{min})/(I_{max} + I_{min})$, where it equals to $(I_{\parallel} - I_{\perp})/(I_{\parallel} + I_{\perp})$. The modulation depths of other two surface gratings are more than 30%, and those of the inner gratings are less than the corresponding surface gratings, 15–22%. Considering that both the fill factors of the gratings and the fabrication parameters were not optimized for THz devices, the modulation depth can be further increased.

Fig. 12 shows the imaging of two polarization directions of Sample s-10 at 2.52 THz. The detector is an uncooled microbolometer array optimized for 0.7-5 THz and one pixel is 17 μm. The modulation depths of Sample s-10 is 40% at 2.52 THz measured by imaging.

The transmittance of the diamond plate is more than 90% at 1.6 THz and the maximum transmittance of Sample s-10 is about 80% (including the influence of the substrate), which were measured by power meter. For other gratings, the modulation depths decrease mainly due to the increase of I_{min}, rather than the decrease of I_{max}, although the fill factors have an influence on the transmittances. Hence, the THz wave may partly transmit in the irradiated region. Both the amplitude modulation and the phase modulation contribute to the modulation depths.

It is needed to point out that the requirements are different between to make micrometer electric wire and to make THz polarizer. The residual single crystal phase in the grating lines (acting as break points) hinders the electrons freely flow through the whole wire, so that the measurement of the electric conductivity will fail. However, the local effective free electron densities in the irradiated region, which can respond to electromagnetic wave, may be higher than the value simply estimated by the conductivity calculated from the voltammetric curve. It is why we can obtain THz polarizers.

The THz data indicates that the transmittance of THz wave can vary in a large range by changing the fabrication conditions although the mechanics of forming THz polarizer of those gratings is not explicit and needs to be deep studied. There will be the interactions (couplings) between layers when we fabricate THz wave modulation devices with 3D structures inside diamond plates. The results encourage us to expect novel THz devices because a changeable electric conductivity provides a new freedom of design.

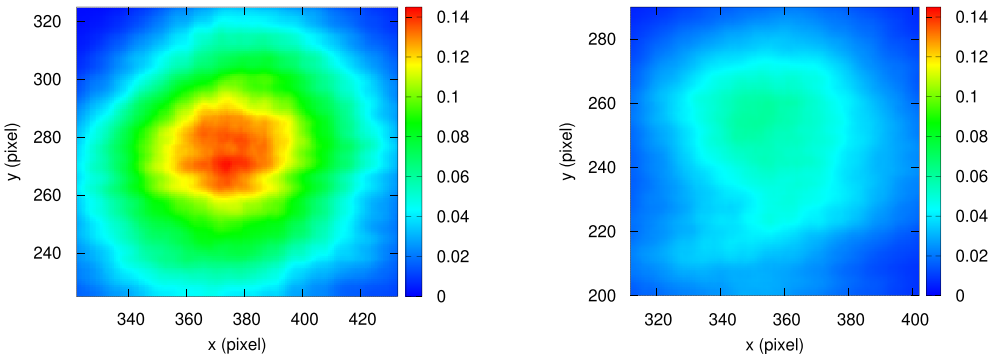

Fig. 12. Terahertz imaging of Sample s-10 at 2.52 THz. The modulation depth is 40%.

5. Conclusion

As our results show, the results shows the electric properties of the irradiated region are very sensitive to the degree of the phase transition. The requirement of writing optical and THz elements are much looser than writing the electric element. The results demonstrated that we can fast fabricate optical gratings and THz polarizers on the surface or inside of the normal grade single crystal diamond plates. Our experimental results also show that we can use normal grade single diamond plates to fabricate the electric elements or the electric circuit on the surface of diamond. In brief, a high repetition fs laser is a powerful rapid processing tool to fabricate electromagnetic wave elements made of diamond material. The sensitivity of the optical and electric properties of the irradiated region just makes novel electromagnetic wave devices with complex 3D structures possible due to couplings between layers.

Declaration of Competing Interest

The authors declare that they have no known competing financial interests or personal relationships that could have appeared to influence the work reported in this paper.

Acknowledgement

This work was supported by National Natural Science Foundation of China, China (NSFC, Grant No. 61827821,11804320).

The authors wish to thank Professor Yang Qu and other members of Institute of Microelectronics of the Chinese Academy of Sciences for helpful discussions about the measurement of the resistivity.

The authors wish to thank Professor Tao Xue of Center for Analysis and Tests, Tianjin University for helpful discussions about the measurement of the Raman spectra.

The authors wish to thank everybody who gave us precious suggestions.

References

[1] L. Balek, M. Buchtova, M. Kunova Bosakova, M. Varecha, S. Foldynova-Trantirkova, I. Gudernova, I. Vesela, J. Havlik, J. Neburkova, S. Turner, M. A. Krzyscik, M. Zakrzewska, L. Klimaschewski, P. Claus, L. Trantirek, P. Cigler, P. Krejci, Nanodiamonds as "artificial proteins": Regulation of a cell signalling system using low nanomolar solutions of inorganic nanocrystals, Biomaterials 176 (2018) 106–121, https://doi.org/10.1016/j.biomaterials.2018.05.030.

[2] V. Zuerbig, W. Pletschen, J. Hees, R. Sah, L. Kirste, N. Heidrich, C. Nebel, O. Ambacher, V. Lebedev, Transparent diamond electrodes for tunable micro-optical devices, Diam. Relat. Mater. 38 (2013) 101–103, https://doi.org/10.1016/j.diamond.2013.06.010.

[3] S. Johnson, P.R. Dolan, J.M. Smith, Diamond photonics for distributed quantum networks, Progress Quant. Electronics 55 (2017) 129–165, https://doi.org/10.1016/j.pquantelec.2017.05.003.

[4] F. Mouhamadali, S. Equis, F. Saeidi, J. Best, M. Cantoni, P. Hoffmann, K. Wasmer, Nanosecond pulsed laser-processing of cvd diamond, Opt. Lasers Eng. 126 (2020), 105917, https://doi.org/10.1016/j.optlaseng.2019.105917.

[5] M. Komlenok, V. Kononenko, V. Ralchenko, S. Pimenov, V. Konov, Laser induced nanoablation of diamond materials, Phys. Procedia 12 (2011) 37–45, https://doi.org/10.1016/j.phpro.2011.03.103.

[6] V.V. Kononenko, I.I. Vlasov, V.M. Gololobov, T.V. Kononenko, T.A. Semenov, A. A. Khomich, V.A. Shershulin, V.S. Krivobok, V.I. Konov, Nitrogen-vacancy defects in diamond produced by femtosecond laser nanoablation technique, Appl. Phys. Lett. 111 (2017), 081101, https://doi.org/10.1063/1.4993751.

[7] Y.-C. Chen, P.S. Salter, S. Knauer, L. Weng, A.C. Frangeskou, C.J. Stephen, S. N. Ishmael, P.R. Dolan, S. Johnson, B.L. Green, G.W. Morley, M.E. Newton, J. G. Rarity, M.J. Booth, J.M. Smith, Laser writing of coherent colour centres in diamond, Nat. Photonics 11 (2017) 77–81.

[8] H. Hanafi, S. Kroesen, L.-M. Georgia, C. Nebel, W.H.P. Pernice, C. Denz, Polycrystalline diamond photonic waveguides realized by femtosecond laser lithography, Opt. Mater. Exp. 9 (2019) 3109–3114.

[9] M. Girolami, A. Bellucci, P. Calvani, S. Orlando, V. Valentini, D.M. Trucchi, Raman investigation of femtosecond laser-induced graphitic columns in single-crystal diamond, Appl. Phys. A 117 (2014) 143–147.

[10] A. Oh, B. Caylar, M. Pomorski, T. Wengler, A novel detector with graphitic electrodes in cvd diamond, Diam. Relat. Mater. 38 (2013) 9–13, https://doi.org/10.1016/j.diamond.2013.06.003.

[11] M. Girolami, L. Criante, F.D. Fonzo, S.L. Turco, A. Mezzetti, A. Notargiacomo, M. Pea, A. Bellucci, P. Calvani, V. Valentini, D.M. Trucchi, Graphite distributed electrodes for diamond-based photon-enhanced thermionic emission solar cells, Carbon 111 (2017) 48–53.

[12] P.S. Salter, M.J. Booth, Ultrafast laser processing of diamond, Proc. of SPIE 8974 (2014) 89740T, https://doi.org/10.1117/12.2040384.

[13] I. Yamada, K. Takano, M. Hangyo, M. Saito, W. Watanabe, Terahertz wire-grid polarizers with micrometer-pitch al gratings, Opt. Lett. 34 (2009) 274–276.

[14] K. Takano, H. Yokoyama, A. Ichii, I. Morimoto, M. Hangyo, Wire-grid polarizer sheet in the terahertz region fabricated by nanoimprint technology, Opt. Lett. 36 (2011) 2665–2667.

[15] Y. Li, D. Pang, W. Liu, Q. Ma, Q. Song, M. Hu, Polarization modulation of terahertz wave by femtosecond laser additive manufactured tin grating, Infrared Phys. Technol. 95 (2018) 76–80.

[16] S. Amoruso, A. Andreone, A. Bellucci, C. Koral, M. Girolami, M. Mastellone, S. Mou, S. Orlando, G.P. Papari, D.P. Abd R, A. Polini, A. Rubano, V. Santagata, V. Serpente, D.M. Valentini, Trucchi,, All-carbon thz components based on laser-treated diamond, Carbon 163 (2020) 197–201, https://doi.org/10.1016/j.carbon.2020.03.023.

[17] D. Wei Zhang, Y. Xiao Cui, Surface chemical modification of cvd diamond films by laser irradiation, Int. J. Refract Metal Hard Mater. 81 (2019) 36–41, https://doi.org/10.1016/j.ijrmhm.2019.02.017.

[18] A.C. Ferrari, J. Robertson, Resonant raman spectroscopy of disordered amorphous, and diamondlike carbon, Physical Review B 64 (2001), 075414, https://doi.org/10.1103/PhysRevB.64.075414.

[19] A.M. Zaitsev, Optical properties of diamond: a data handbook, Springer, 2001.

[20] M.A. Prelas, G. Popovici, L.K. Bigelow, Handbook of industrial diamonds and diamond films, CRC Press, 1997.

[21] A.C. Ferrari, J. Robertson, Interpretation of raman spectra of disordered and amorphous carbon, Phys. Rev. B 61 (2000) 14095–14107.

[22] C. Pardanaud, C. Martin, P. Roubin, G. Giacometti, C. Hopf, T. Schwarz-Selinger, W. Jacob, Raman spectroscopy investigation of the h content of heated hard amorphous carbon layers, Diam. Relat. Mater. 34 (2013) 100–104, https://doi.org/10.1016/j.diamond.2013.02.009.

[23] A. Dychalska, P. Popielarski, W. Franków, K. Fabisiak, K. Paprocki, M. Szybowicz, Study of cvd diamond layers with amorphous carbon admixture by raman

scattering spectroscopy, Mater. Sci.-Poland 33 (2015) 799–805, https://doi.org/10.1515/msp-2015-0067.
[24] L. Chen, X. Miao, H. Ma, L. Guo, Z. Wang, Z. Yang, C. Fang, X. Jia, Synthesis and characterization of diamonds with different nitrogen concentrations under high pressure and high temperature conditions, CrystEngComm 20 (2018) 7164–7169, https://doi.org/10.1039/c8ce01533c.
[25] X. Li, H.-K. Mao, Solid carbon at high pressure: Electrical resistivity and phase transition, Phys. Chem. Minerals 21 (1994) 1–5.